MDPI

Article

Estimation of Water Interception of Winter Wheat Canopy Under Sprinkler Irrigation Using UAV Image Data

Xueqing Zhou, Haijun Liu * and Lun Li

Beijing Key Laboratory of Urban Hydrological Cycle and Sponge City Technology, College of Water Sciences, Beijing Normal University, Beijing 100875, China; zhouxueqing2001@126.com (X.Z.); 202021470021@mail.bnu.edu.cn (L.L.)
* Correspondence: shanxilhj@bnu.edu.cn; Tel.: +86-136-81334108

Abstract: Canopy water interception is a key parameter to study the hydrological cycle, water utilization efficiency, and energy balance in terrestrial ecosystems. Especially in sprinkler-irrigated farmlands, the canopy interception further influences field energy distribution and microclimate, then plant transpiration and photosynthesis, and finally crop yield and water productivity. To reduce the field damage and increase measurement accuracy under traditional canopy water interception measurement, UAVs equipped with multispectral cameras were used to extract in situ crop canopy information. Based on the correlation coefficient (r), vegetative indices that are sensitive to canopy interception were screened out and then used to develop canopy interception models using linear regression (LR), random forest (RF), and back propagation neural network (BPNN) methods, and lastly these models were evaluated by root mean square error (RMSE) and mean relative error (MRE). Results show the canopy water interception is first closely related to relative normalized difference vegetation index ($R_{\triangle NDVI}$) with r of 0.76. The first seven indices with r from high to low are $R_{\triangle NDVI}$, reflectance values of the blue band (Blue), reflectance values of the near-infrared band (Nir), three-band gradient difference vegetation index (TGDVI), difference vegetation index (DVI), normalized difference red edge index (NDRE), and soil-adjusted vegetation index (SAVI) were chosen to develop canopy interception models. All the developed linear regression models based on three indices ($R_{\triangle NDVI}$, Blue, and NDRE), the RF model, and the BPNN model performed well in canopy water interception estimation (r: 0.53–0.76, RMSE: 0.18–0.27 mm, MRE: 21–27%) when the interception is less than 1.4 mm. The three methods underestimate the canopy interception by 18–32% when interception is higher than 1.4 mm, which could be due to the saturation of NDVI when leaf area index is higher than 4.0. Because linear regression is easy to perform, then the linear regression method with NDVI is recommended for canopy interception estimation of sprinkler-irrigated winter wheat. The proposed linear regression method and the $R_{\triangle NDVI}$ index can further be used to estimate the canopy water interception of other plants as well as forest canopy.

Keywords: canopy interception; UAV; multispectral image data; vegetation indices; model performance

1. Introduction

Canopy water interception is the water amount that is intercepted then stored for a while in the canopy of a plant, tree, or bush during rainfall or sprinkler irrigation, and a key component in the land water cycle [1]. The canopy water interception has been measured from 10% to 50% of total rainfall in different types of forest [2,3], 7–36% in crops [4], and 10–40% in bushes [5]. The large variations in canopy interception depend on plant and forest species and growth characteristics. Compared to the natural forest and bush ecosystems, the sustainable development of farmland systems mainly depends on irrigation, especially in semiarid and arid regions. The North China Plain (NCP) is one of the main grain production regions in China, producing approximately 60% of wheat and 25% of maize of China's total amount [6]. Most wheat in the NCP is irrigated because

the precipitation (approximately 150 mm) cannot meet the wheat ET of approximately 450 mm [7,8]. Sprinkler irrigation has now been increasingly used to irrigate wheat fields in the NCP to reduce the labor cost and improve field water and nutrient conditions by combining with the fertigation system [9]. Unlike the surface and drip irrigation methods, a part of sprinkler irrigation water can be intercepted by crop canopy, which then influences the irrigation water distribution and water use efficiency [10]. The evaporation of canopy interception further influences the field energy balance and microclimate, then crop physiological function of photosynthesis and transpiration, and finally crop yield and evapotranspiration [11–14]. Therefore, quantifying the canopy water interception under sprinkler irrigation is critical to understanding the mechanism of crops response to field microclimate change, crop evapotranspiration, and water use efficiency.

The used methods for canopy water interception include direct and indirect methods. Most indirect methods are based on water balance theory. For indirect method measurement, water collectors are placed above and under the plant canopy, and the canopy interception is determined as the water difference in the collectors between above and under the canopy. By using the water balance method, the canopy interception was measured at 2.9–4.7 mm for wheat [15], 1.1–2.31 mm for maize [1,16], and 0.8–7.6 mm for soybean [17]. Because the stem flow water is not considered in the water balance method, therefore the measured water interception is overestimated. The wiping water method is directly collecting water on the canopy and then can get a much more accurate canopy interception amount. For example, Kang, Wang [10] used the wiping method within the wheat field under sprinkler irrigation and reported that the canopy interception varied from 0.3 to 1.0 mm with an average of 0.6 mm when the wheat leaf area index (LAI) is 2.3–6.7. Compared to the wiping method, the water balance method greatly overestimates the canopy interception. Liu, Chang [18] measured the stem flow of wheat and found it is approximately 30% of the irrigation water above the canopy. When the stem flow water is considered in the water balance method, the canopy interception ranges from 0.6 to 1.3 mm with an average of 0.9 mm, which is close to the amount (0.6 mm) using the wiping method. Both the wiping method and improved water balance method can accurately determine the canopy interception of plants in the field, while they are time consuming and show great variations among the samples. Further, both methods could destroy plants in the field, and then the measurement cannot be repeated in the same place with the same plants, so the uncertainty of the results is increased. Therefore, an improved water balance method was used to get the real canopy interception data in the study. The advantage of the improved method over the traditional one is that it measures the water amounts on all stems, leaves, ears, and shoots, effectively avoiding the risk of overestimating canopy interception. Although this method also causes damage to crops, it provides more accurate data, thus facilitating the acquisition of a more accurate model.

Unmanned aerial vehicles (UAVs) combined with professional equipment (for example, multispectral cameras and sensors, etc.) could implement the aim of in situ data acquisition/perception, decision making, and action performance [19]. In comparison with traditional remote sensing technologies (such as satellites and manned airborne systems), UAVs possess technological advancement, high efficiency, low cost, and the ability to perform real-time actions [20]. Therefore, the UAVs have been widely used in all walks of life. In the agriculture industry, the UAVs equipped with multispectral sensors are able to perform high-precision monitoring of canopy characteristics over large areas [21]. A series of spectral index and spectral derivative models have been developed to estimate the water content of different crops [22,23]. Ceccato [24] and Mohammad et al. [25] reported that near-infrared (Nir) and shortwave infrared (SWIR) are the more ideal bands for studying the vegetation water changes. Liu et al. [26] constructed a water sensitivity index using hyperspectral data, and the results showed that the near infrared shoulder region spectral ratio index (NSRI) is a suitable vegetation index for wheat water content estimation. However, there are fewer research reports on canopy water interception using UAV technologies, especially timely and precise monitoring of the canopy interception

under sprinkler irrigation conditions. Rainfall and snow interception in forests or shrubs have been estimated using unmanned aerial vehicles (UAVs) technology and satellite remote sensing data [27,28]. To date, research on estimating canopy interception of winter wheat under sprinkler irrigation using multispectral technology is limited. One of the major challenges is the lack of reliable indices. Although various vegetation indices (such as NDVI, SAVI, Vogelmann Red Edge Index 1, and so on) have been tested in studies, none have been identified that reflect canopy interception accurately and immediately, and the selected indices show instability across different vegetation types and environments [29]. Another challenge is that no good algorithms are developed. Most models at present are based on complex physical processes and remote sensing data, which greatly reduces the convenience of timely estimating canopy interception [27]. Thus, further improvement of multispectral technology for canopy interception estimation is crucial.

For improving the accuracy of crop canopy monitoring and fusing remote sensing data from various bands, three regression algorithms—linear regression (LR), random forest (RF), and back propagation neural network (BPNN)—have been widely used [30]. The LR method effectively captures the direct relationship between predictor and response variables, with a simple underlying principle and wide applicability. Liu et al. [31] demonstrated the feasibility of using the RF and BPNN methods to analyze canopy interception because this approach has the advantage of effectively capturing the nonlinear relationships between remote sensing data features and crop phenotypes while being relatively unaffected by noise and the number of input variables [32]. Therefore, the three methods of LR, RF, and BPNN could be employed to develop prediction models of water canopy interception using multispectral data.

In this study, UAVs equipped with multispectral cameras were used to get multispectral images of winter wheat canopy after sprinkler irrigation; then, parameters were calculated using the multispectral images data and screened out based on the correlation coefficient with the measured canopy water interception. Lastly, the prediction models of winter wheat canopy interception based on unary, multivariate linear regression, random forest, and back propagation neural network algorithms were developed and evaluated. The results in this study could help researchers and water resource managers timely and precisely determine the in situ canopy water interception in farmland and forests using UAV technology.

2. Materials and Methods

2.1. Overview of the Study Area and Experiment

The experiment was carried out in April and May in winter wheat growth periods in 2021 and 2022 at Dacaozhuang National Seed Experiment Station (37°29′49.25″ N, 114°55′40.59″ E, altitude 26 m) in Ningjin County, Xingtai City, Hebei Province, China (Figure 1). The study region is located on the North China Plain (NCP) with a warm temperate semi-arid monsoon climate. The average annual precipitation is 430 mm, with around 60–70% occurring between June and September. The average annual temperature is 13 °C, the average sunshine duration is 2428 h, and the frost-free period is about 250 d [33].

The winter wheat experimental field is 200 m long from north to south and 60 m wide. The solid-set sprinkler irrigation system [34] is widely used to irrigate winter wheat and was then used in this study. Three pipe laterals were deployed along the long side of the field, with the distances to the west field edge of 12, 30, and 48 m, respectively. The spacing between pipe laterals was 18 m. Impact sprinklers (model PXS20-D, Tonghua Zhenyu Sprinkler Irrigation Equipment Factory, Zhengzhou, China) were mounted on 1.1 m height risers and approximately 0.4 m higher than the wheat canopy when the wheat reached its full height of approximately 0.8 m. The discharge of the sprinkler is 2.2 m^3 h^{-1} under the normal working pressure of 0.25 MPa. The spacing between sprinklers is 18 m. In this sprinkler irrigation arrangement, the intensity of irrigation is 7 mm h^{-1}. The Christiansen coefficient [35] of the sprinkler water distribution was 0.8 and higher than the

lowest requirement of 0.75 in the Chinese sprinkler irrigation standard [36], indicating the sprinkler irrigation system is in normal working condition.

The winter wheat variety of Yingbo 700 was used with sowing spacing of 20 cm. The sowing rate was 100 and 120 kg ha^{-1} on October 20 and 30 in 2021 and 2022, respectively. The wheat was harvested on June 10 in both wheat seasons. The measured wheat yields in the 2021 and 2022 seasons were 9.75 and 9.34 t ha^{-1}, respectively, which are higher than the mean yield of 7.49 t ha^{-1} reported by the local government (Hebei Bureau of Statistics data, http://www.hetj.gov.cn/hbstjj/ (accessed on 30 October 2024)).
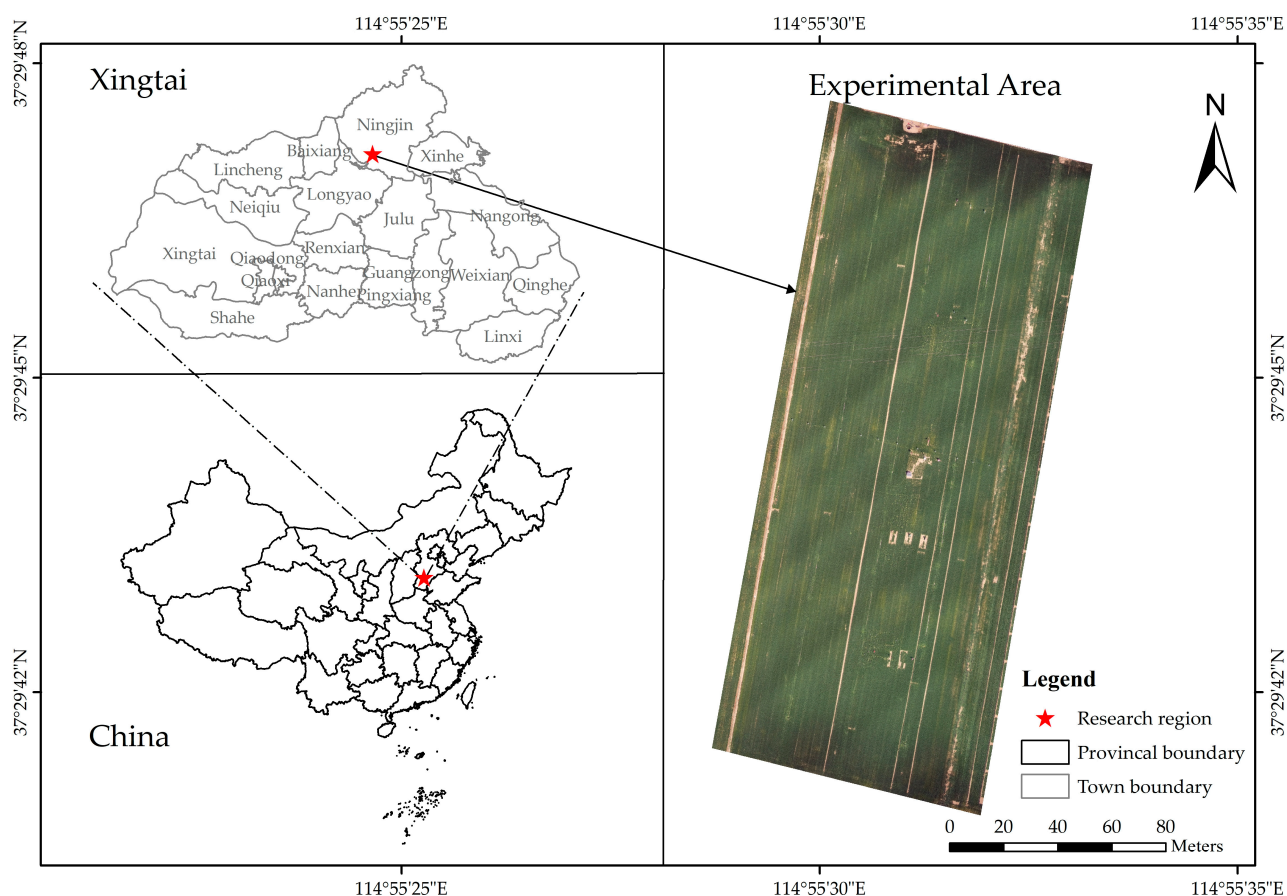
Figure 1. Map of experimental location and experimental field in this study.

2.2. Canopy Water Interception Measurement

During the two-year experiment period (2021 and 2022 wheat seasons), a total of four canopy interception measurements after sprinkler irrigation events were conducted on May 6 and 23 in 2021 and April 25 and May 16 in 2022. The main environmental data for the day of the experiment are shown in Table 1. The four measurements are referring to Test A, Test B, Test C, and Test D, respectively. In each measurement, three subplots with a size of 18 m × 18 m for each were chosen. The experiments were mostly conducted in the morning and midday. After approximately 4–5 h of sprinkler irrigation, the wheat canopy was fully wetted, and the canopy water interception reached its maximum capacity. One-quarter of the experimental plot was selected for canopy interception measurement to minimize the influence of field measurement on the wheat plants surrounding the measurement sites.

Table 1. The main environmental data for the day of the experiment.

Test Name	Date	Total Radiation	Relative Humidity	Average Air Temperature	Maximum Temperature	Minimum Temperature	Average Wind Speed
		$MJ \times m^{-2} \times d^{-1}$	(%)	(°C)	(°C)	(°C)	(m/s)
Test A	6 May 2021	23.42	41.42	21.83	30.64	14.69	3.38
Test B	23 May 2021	20.84	67.70	20.66	26.35	16.79	2.46
Test C	25 April 2022	15.94	85.30	21.24	27.86	15.56	1.34
Test D	16 May 2022	29.97	53.42	19.21	28.18	9.01	1.31

Canopy water interception was defined as the variation in canopy masses pre- and post-sprinkler irrigation. The measurement procedure involved the following steps: (1) ascertaining canopy water content of wheat before irrigation: firstly, around 20 wheat stems were severed at the stem base near ground surface, then the total fresh and oven-dried masses of the 20 stems were gauged, and finally the water content (θ) of the fresh plant was calculated as $\theta = \frac{fresh\ mass - dry\ mass}{dry\ mass}$; (2) clearing stems around the measurement sites, at each selected site, plants within a 15 cm length row were retained, while other plants, spaced 20 cm from the selected samples, were cut to minimize their impact on the plant samples' measurement; (3) determining the wet biomass of the sampled stems in the 15 cm length row, after sprinkler irrigation, the plant samples were immediately covered with large plastic bags (0.6 m in width and 0.8 m in height) from top to bottom and cut at the stem base, then the bags were tightly sealed once all plants were placed inside; finally, the total wet stem mass ($W1$, g) was measured using a 0.01 g precision balance; (4) determining the dry mass of the sampling stems in the 15 cm length row, the number (n) of the sampled plants in the 15 cm length row was recorded, then all plants were dried in an oven and the dry mass were measured as W_2 (g); (5) determining the total canopy water interception in the sampling stems, assuming the water content of plants remains unchanged pre- and post-sprinkler irrigation, the total canopy water interception ($W3$, g) is represented by the increase in mass following sprinkler irrigation, and was calculated by the equation $W_3 = W_1 - (1 + \theta)W_2$; (6) last, determining the canopy interception depth (CI, mm) following a sprinkler irrigation in the field, it was calculated as $CI = 10^{-3} * \frac{W_3}{n} N$, where N is the plant density, plants m^{-2}.

The leaf area index (LAI) in each canopy interception measurement site was determined. Twenty stems were chosen, and every leaf thereon was detached, and the entire leaf area (LA, cm^2) was gauged with the LI-3000C portable leaf area meter (LI-COR, Inc., Lincoln, NE, USA). Then the LAI was calculated as $LAI = 10^{-4} * \frac{LA}{20} N$, where LA is the total active leaf area of the sampled plants in cm^2, and N is the plant density in plants m^{-2}.

2.3. UAV Image Acquisition and Processing

A UAV system (model DJI P4 Multispectral Version, Dajiang Innovation Technology Co., Ltd., Shenzhen, China) was used to collect high temporal and spatial resolution multispectral images and RGB images in the experimental area. The P4 UAV system is equipped with a multispectral camera, which has one visible light imaging sensor channel and five multispectral imaging channels, namely blue (450 ± 16 nm), green (560 ± 16 nm), red (650 ± 16 nm), red edge (730 ± 16 nm), and near infrared (840 ± 16 nm). Six images were obtained in one shot, and the effective pixels of each image are approximately 2 million. Flight height above ground surface was set to 50 m, and the acquisition period was between 11:00 and 15:00 under the circumstances of clear and cloudless weather. The multispectral image data of the entire test area were collected prior to each irrigation as background values. Immediately after each sprinkler irrigation, the multispectral image data in the three subplots with canopy interception measurement were obtained.

The multispectral images were calibrated using a standard reflectance calibration panel [37]. The Pix4D mapper (Pix4D, Prilly, Switzerland), a specialized processing software for processing UAV aerial photograph data, was employed to perform orthorectification

and image stitching on the acquired images [38]. As a result, a single-band orthophoto with a ground resolution of 3.52 cm per pixel, along with RGB images, was obtained. During remote sensing image acquisition, due to the limitations of the equipment itself and the influence of soil background on plant canopy reflectance spectra [39], the pre-processing of soil background rejection was performed on the multispectral images. ENVI 5.3 software (Exelis Visual Information Solutions, Broomfield, CO, USA) was utilized to distinguish winter wheat from non-vegetation (including soil and other features) by applying a threshold segmentation method based on the differences in reflectance among the various bands between winter wheat and soil. In ArcMap 10.5 software (ESRI, California, CA, USA), buffer zones were built around the sampling points, with a 1 m^2 area generation, which were distributed in relatively uniform positions around the sampling point. Afterwards, the mean reflectance value of all raster cells within each buffer zone was computed and taken as the reflectance value for the corresponding sampling point [40]. Reflectance data of 48 sampling points per test were obtained via this procedure. The vegetation indices were calculated using the band math function in ENVI 5.3, which used the same extraction method of the reflectance value of the respective sample points.

2.4. Vegetation Indices Calculation

The vegetation spectral index, a dimensionless parameter, is formed by linearly or non-linearly combining the reflectance of different bands of remote sensing images based on vegetation spectral absorption characteristics. Furthermore, the combination of reflectance from multiple bands can mitigate the influence of leaf physical properties, such as structure, orientation, and radiation angle, on canopy spectra. Therefore, vegetation spectral index can provide a simple and effective measure of the vegetation status of the plant canopy. In this study, seven vegetation indices (VIs) that have shown good performance in predicting canopy water status and reflecting the characteristics of vegetation canopy were selected. They are the difference vegetation index (DVI), normalized difference red edge index (NDRE), soil adjusted vegetation index (SAVI), three-band gradient difference vegetation index (TGDVI), normalized difference vegetation index (NDVI), normalized difference water index (NDWI), and relative normalized difference vegetation index (R$_{\triangle NDVI}$) (Table 2). The calculation equations are also listed in Table 2. The NDVI index is widely used for monitoring plant growth and correcting specific radiometric errors with ranges from −1 to 1 [41]. We found in the experiment that there are obvious variations in NDVI in the sprinkler-irrigated and no-irrigated canopy. Then we calculated the relative normalized difference vegetation index (R$_{\triangle NDVI}$) as a vegetation spectral index for canopy interception estimation.

Table 2. The selected vegetation spectral index and corresponding calculation formula.

Vegetation Index	Abridge	Formula	Literature Sources
Difference vegetation index	DVI	$\text{Nir} - \text{Red}$	[42]
Normalized difference red edge index	NDRE	$(\text{Nir} - \text{Red Edge})/(\text{Nir} + \text{Red Edge})$	[43]
Soil-adjusted vegetation index	SAVI	$(1 + L) \times (\text{Nir} - \text{Red})/(\text{Nir} + \text{Red} + L)$	[44]
Three-band gradient Difference vegetation index	TGDVI	$(\text{Nir} - \text{Red})/(\lambda_{\text{Nir}} - \lambda_{\text{Red}}) - (\text{Red} - \text{Green})/(\lambda_{\text{Red}} - \lambda_{\text{Green}})$ (If TGDVI < 0, then TGDVI = 0)	[45]
Normalized difference Vegetation index	NDVI	$(\text{Nir} - \text{Red})/(\text{Nir} + \text{Red})$	[41]
Normalized difference water index	NDWI	$(\text{Green} - \text{Nir})/(\text{Green} + \text{Nir})$	[46]
Relative normalized Difference vegetation index	R$\triangle$NDVI	$(\text{NDVI2} - \text{NDVI1})/\text{NDVI1}$	This study

Note: Nir: reflectance values of near-infrared band; Red: reflectance values of red band; Blue: reflectance values of blue band; Green: reflectance values of green band; Red Edge: reflectance values of red edge band; L is taken as 0.5, and λ is the wavelength; NDVI$_1$ is the NDVI value of the winter wheat canopy before the start of sprinkler irrigation; and NDVI$_2$ is the NDVI value of the winter wheat canopy immediately measured after sprinkler irrigation.

2.5. Model Development

The quality of the spectral data in Test B was poorer than that of the other three experiments due to the influence of weather and clouds during collection and was removed in the following data analysis. Based on Tests A, C, and D, a total of 128 sets of canopy interception water samples were selected, along with corresponding values of vegetation indices and single-band reflectance. Seventy-five percent of the samples were randomly chosen for model development and the remaining 25% for model validation. Three methods, including linear regression, random forest, and backpropagation neural network, were applied to develop the canopy interception model using the vegetation indices listed in Table 2.

2.5.1. Linear Regression

A linear regression model predicts a response variable as a linear function of one or more predictor variables, encompassing both unary (ULR) and multivariate (MLR) linear regression. In unary linear regression, it is assumed that there exists a linear relationship between the dependent and independent variables, which can be represented by a straight line. The best-fitting line is determined by minimizing the sum of the squared residuals, thereby minimizing the error between the predicted values and the actual observations. Multiple linear regression is a commonly employed statistical model used to predict a continuous dependent variable based on several independent variables, which enhance the complexity and accuracy of the predictive model [47]. To assess the applicability and accuracy of MLR models, it is crucial in practice to carry out regression diagnostics and model validation [48]. The ULR and MLR models in this study were developed using Origin 2022 software (OriginLab Co., Northampton, MA, USA).

2.5.2. Random Forest Model (RF)

The random forest (RF) model is an integrated machine learning algorithm for classification or regression prediction, which is characterized by high robustness and high learning ability [49]. It is an integrated learning algorithm based on decision trees. It randomly selects M subsets of N samples from N training samples by the bootstrap sampling method in a releasing manner and trains a decision tree for each subset individually and takes the average of the prediction results of M decision trees as the output value of regression random forest [50]. After multiple training and optimization of the model by incrementally increasing the minimum number of leaves nodes starting from the default value of one to mitigate over-fitting, finally the decision tree of the canopy interception model was set to 100 (default), with the minimum number of leaves nodes being 6. All modeling processes and analyses of the RF model were conducted using MATLAB R2020a software (Math Works, Natick, MA, USA).

2.5.3. Back Propagation Neural Network (BPNN)

The backpropagation neural network (BPNN) is a type of artificial neural network that utilizes an error backpropagation algorithm. Its fundamental architecture consists of an input layer, one or more hidden layers, and an output layer. By integrating multiple layers of neurons, BPNN is capable of establishing a nonlinear mapping relationship. This network can approximate the nonlinear relationship between inputs and outputs by adjusting the weights and biases of the hidden layers [51]. The hidden layer transfer function of the BPNN model was set as TANSIG, and the Levenberg–Marquardt (L–M) algorithm was used as the network training function based on numerical optimization theory [23].

The BPNN method in MATLAB R2020a software was applied to develop canopy interception prediction models. The quantity of neurons within the hidden layer is computed in accordance with the subsequent empirical formula [52]:

$$N = \sqrt{n + m} + a \ (0 < a \leq 10) \tag{1}$$

where N, n, and m are the numbers of nodes in the hidden, input, and output layers, respectively, and a is the empirical value. In the study, the input layer consists of seven nodes, while the output layer contains one node. According to Equation (1), the range of nodes within the hidden layer is defined to be between 1 and 12. The model performance testing began with a hidden layer neuron count of 1, increasing incrementally, and ultimately the number of hidden layer nodes was set to 12, the maximum number of iterations was 100, and the learning rate was 0.01.

2.6. Model Evaluation

All developed models were evaluated using three indicators: coefficient of determination (R^2), root mean square error (RMSE), and mean relative error (MRE) [53].

When R^2 approaches 1, both RMSE and MRE approach 0, indicating superior model estimation performance. The accuracy parameters of the models were statistically compared in this study to identify the optimal model intuitively.

2.7. Figure Preparation

All data were processed in Microsoft Excel. The correlation relationship between canopy interception and vegetation indices and all figures were prepared using the Origin 2022 software (OriginLab Co., Northampton, MA, USA).

3. Results and Analysis

3.1. Correlation Analysis Between Canopy Water Interception and Vegetation Spectral Indices

The correlation relationship between measured canopy interception and the seven vegetation indices and five-band reflectance (Blue, Green, Red, Red Edge, and Nir) was analyzed, and the results are shown in Figure 2. The correlation coefficient is the highest (0.76) for index $R_{\triangle NDVI}$, followed by Blue, Nir, TGDVI, DVI, NDRE, and SAVI, with the corresponding correlation coefficients from 0.43 to 0.33. A correlation coefficient greater than 0.3 shows moderate and strong correlation [54]. Then the seven vegetation indices ($R_{\triangle NDVI}$, Blue, Nir, TGDVI, DVI, NDRE, and SAVI) were used to develop the canopy water interception models by the linear regression model (Section 3.2), random forest regression model (Section 3.3), and BP neural network regression model (Section 3.4).
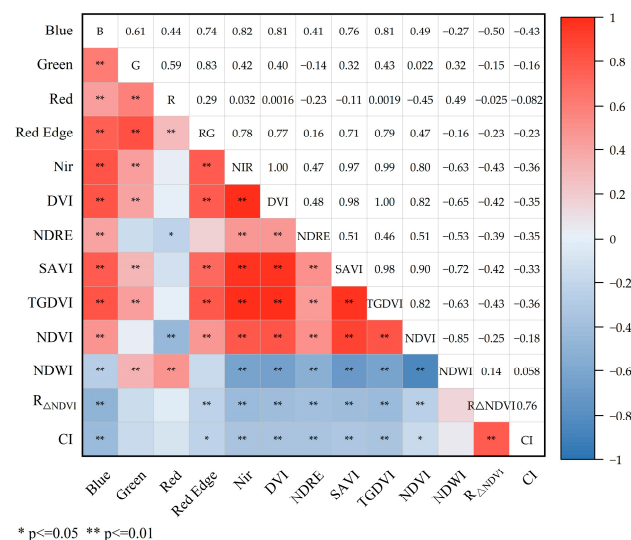

* p<=0.05 ** p<=0.01

Figure 2. Heat map of correlation analysis between vegetation indices and canopy water interception. Note: * indicates the correlation coefficient between the two indices is significant at 0.05 level; ** indicates the relationship is significant at 0.01 level.
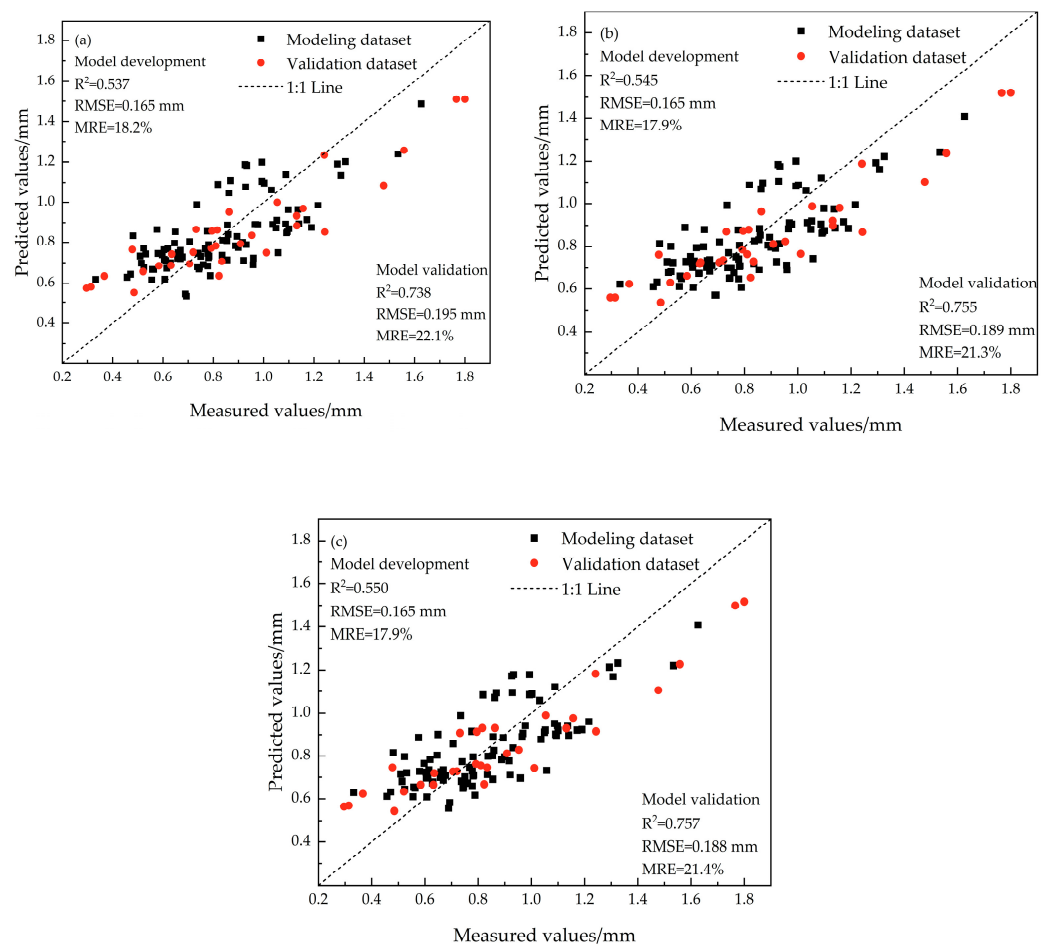
3.2. Linear Regression Model

The unary and multivariate linear regression models are fitted to estimate canopy water interception after sprinkler irrigation using the seven vegetation indices selected in Section 3.1. Table 3 presents the results of the fitted unary and multivariate linear models. Figure 3 shows the performance of three linear regression models using single, two, and three vegetative indices. Based on the results of the single-parameter unary linear regression, the model based on $R_{\triangle NDVI}$ has the optimal fitting performance, with the maximum determination coefficient (R^2) of 0.537 in the model developing process and 0.738 in the model validation process, the corresponding root mean square errors (RMSE) of 0.165 and 0.195 mm, and the average relative errors (MRE) of 18.2% and 22.1% (Figure 3a). The SAVI-based unary linear regression model has the least R^2 in model development (0.031) and the validation process (0.054) and the highest RMSE of 0.239 and 0.371 mm. The other linear regression models with a single vegetation index have R^2 values between 0.04 and 0.12, RMSE values between 0.23 and 0.24 mm, and MRE values between 23 and 24% in the model development process, and 0.05 and 0.21, 0.36 and 0.37 mm, and approximately 37% in the model validation process, respectively.

For the linear regression with two vegetation indices, the fitted model based on $R_{\triangle NDVI}$ and Blue (model 8 in Table 3) has the highest R^2 (0.755), the low RMSE (0.189 mm) and MRE (21.3%) in the model validation process (Figure 3b). The multivariate linear regression model based on three vegetation indices of Blue, NDRE, and $R_{\triangle NDVI}$ (model 11 in Table 3) has the highest R^2 (0.757), the low RMSE (0.188 mm), and MRE (21.4%) in the model validation process (Figure 3c). Compared to the unary linear regression model based on $R_{\triangle NDVI}$ (model 7 in Table 3), multivariate linear regression models (models 8–11 in Table 3) do not greatly improve the accuracy of canopy interception estimation based on the statistical results (R^2, RMSE, and MRE) of models (Table 3).

Table 3. Statistical results of fitted linear models of winter wheat canopy interception using different vegetation indices.

| Model No.	Vegetation Index Used	Regression Function	Model Development			Model Validation		
			R^2	RMSE/mm	MRE/%	R^2	RMSE/mm	MRE/%
1	Blue	* $y = -20.670x_1 + 1.441$	0.124	0.227	22.7%	0.210	0.339	34.2%
2	Nir	$y = -0.506x_2 + 1.124$	0.044	0.237	24.1%	0.078	0.366	37.3%
3	DVI	$y = -0.311x_3 + 1.091$	0.039	0.238	24.2%	0.072	0.367	37.4%
4	SAVI	$y = -0.529x_4 + 1.289$	0.031	0.239	24.6%	0.054	0.371	37.5%
5	NDRE	$y = -1.058x_5 + 1.175$	0.121	0.228	22.9%	0.122	0.357	36.9%
6	TGDVI	$y = -0.0564x_6 + 1.106$	0.040	0.238	24.1%	0.069	0.368	37.3%
7	$R_{\triangle NDVI}$	$y = 10.455x_7 + 0.503$	0.537	0.165	18.2%	0.738	0.195	22.1%
8	Blue, $R_{\triangle NDVI}$	$y = -5.493x_1 + 9.960x_7 + 0.680$	0.545	0.165	17.9%	0.755	0.189	21.3%
9	NDRE, $R_{\triangle NDVI}$	$y = -0.337x_5 + 9.916x_7 + 0.629$	0.548	0.164	17.9%	0.749	0.191	21.7%
10	Blue, NDRE	$y = -13.962x_1 - 0.696x_5 + 1.469$	0.164	0.223	22.0%	0.233	0.334	34.0%
11	Blue, NDRE, $R_{\triangle NDVI}$	$y = -3.276x_1 - 0.266x_5 + 9.735x_7 + 0.708$	0.550	0.165	17.9%	0.757	0.188	21.4%

* Note: "x" in the regression functions is the independent variable, and the subscript numbers 1–7 in "x" represent the indices of blue band (Blue), near-infrared band (Nir), difference vegetation index (DVI), soil adjusted vegetation index (SAVI), normalized difference red edge index (NDRE), three-band gradient difference vegetation index (TGDVI), and relative normalized difference vegetation index ($R_{\triangle NDVI}$) in sequence. "y" refers to the dependent variable and represents the estimated value of canopy interception.

Figure 3. Performance of linear regression models using unary and multiple vegetative indices. Panel (**a**) represents the linear model based on $R_{\triangle NDVI}$ (model 7 in Table 3); (**b**) represents the model based on $R_{\triangle NDVI}$ and Blue (model 8 in Table 3); (**c**) represents model based on $R_{\triangle NDVI}$, Blue, and NDRE (model 11 in Table 3).

### 3.3. Random Forest Regression Model

Vegetation indices with the first seven high correlation coefficients (Figure 2), $R_{\triangle NDVI}$, TGDVI, Blue, Nir, TGDVI, DVI, NDRE, and SAVI, were selected for model development. In order to avoid over-fitting in model training, all seven parameters were employed as the feature input to train the RF regression model. The results show that model R^2 in the model-developing and validating process was 0.738 and 0.533; in turn, the corresponding RMSE were 0.123 and 0.261 mm, and MRE were 12.2% and 25.9% (Figure 4). However, it should be noted that the canopy interception is underestimated by 31.9% when the canopy interception is higher than 1.4 mm (the points inside the ellipse on Figure 4).
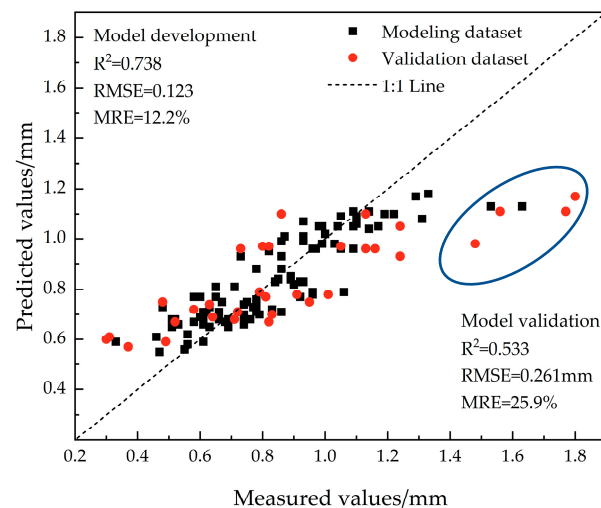
Figure 4. The estimated and measured canopy interceptions by RF model in the model developing and calibrating processes.

3.4. BP Neural Network Regression Model

The BPNN model for canopy interception estimation was trained based on the indices of $R_{\triangle NDVI}$, TGDVI, Blue, Nir, TGDVI, DVI, NDRE, and SAVI. Figure 5 shows the estimated and measured canopy interception in the model training and validation process. Results show that the R^2 in the model training process was 0.691, RMSE is 0.122 mm, and MRE is 14.0%. In the model validation process, the R^2, RMSE, and MRE are 0.667, 0.220 mm, and 24.0%, respectively. The high R^2 and small MRE in the model validation process indicate that the developed BPNN model could accurately estimate canopy interception.
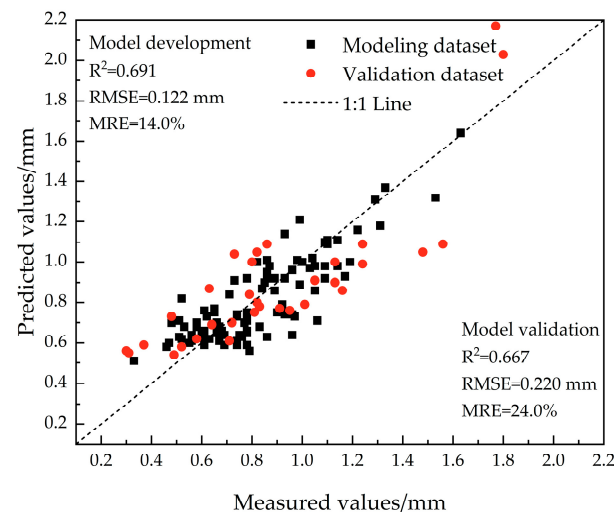
Figure 5. The estimated and measured canopy interceptions by BP neural network model in the model developing and calibrating processes.

4. Discussion

Canopy interception in sprinkler-irrigated fields is not only a key component in water balance analysis but also a key factor that influences canopy energy balance and field microclimate. Previous research indicated that the canopy water interception of winter wheat varies between 0.59 and 1.33 mm and is influenced by sprinkler droplets, wind speed, and leaf area index [10,55,56]. The canopy interception for a mean LAI of 4.76 in this study is between 0.30 and 1.80 mm. The large variation range (0.3–1.8 mm) of canopy interception could be due to the variation in wind speed (1.3–3.4 m s^{-1}), LAI at different measurement

sites (2.8–9.3), and droplet distribution along the jet radius. The mean canopy interception value is 0.63 mm, which is close to the reported mean canopy water interception value of 0.60 mm by Kang [10]. This shows the canopy interception value presented in this study is reliable. Therefore, we developed models based on the measured canopy interception data.

The UAV, equipped with a multispectral camera, could timely sense the changes of land surface and therefore is used to extract canopy characteristics. The results in this study show that the vegetation [10,55,56] indices $R_{\triangle NDVI}$ are highly correlated with canopy interception, with correlation coefficients of 0.76 (Figure 2). The reason could be that the calculation of NDVI takes into account the near-infrared and red-light spectral characteristics, which two are sensitive to plant characteristics [57]. It is reported that the red and near-infrared light band are strongly correlated with vegetation parameters of LAI and canopy cover [58,59]. Moreover, H. H. Bulcock [29] evaluated the feasibility of using NDVI, SAVI, and the Vogelmann Index to estimate LAI and canopy interception in afforested areas and suggested that NDVI is a viable option for estimating canopy interception, which is similar to this study. Considering the NDVI variation with land surface, we suggest using the relative change in NDVI ($R_{\triangle NDVI}$) before and after sprinkler irrigation or rainfall to estimate canopy water interception.

In this study, three methods—univariate and multivariate linear regression, BP neural network, and random forest methods—were developed to estimate canopy interception of winter wheat under sprinkler irrigation based on five vegetation indices and two-band reflectance. Results show that the models developed with the three methods (models 7, 8, and 11 in Table 3, the RF model, and BPNN model) have close values of model evaluation parameters (R^2, RMSE, and MRE). According to the model validation process, the accuracy of the three linear regression models is generally better than that of the BPNN model and RF model. The reason may be attributed to the obvious linear relationship between the index $R_{\triangle NDVI}$ and canopy water interception. Due to the high capabilities for processing complex nonlinear relationships, the BP neural network and RF methods models, which usually require a large quantity of data for training and use complex algorithms [60,61], have been successfully applied in predicting crop biomass and yield [62], assessing crop health [23], and estimating canopy water content [63]. Regarding the linear relationship between the vegetation index and canopy interception, the nonlinear characteristics of BPNN and RF models may lead to over-fitting [64] or performance degradation, especially when the sample size of the data is insufficient. The three methods of linear regression, RF, and BPNN models performed well for estimating canopy water interception of winter wheat when canopy interception is less than 1.4 mm, then show large errors for canopy interception larger than 1.4 mm. The linear models and RF model underestimated the canopy interception by 18.0% and 31.9%, in turn (Figures 3 and 4), and the BPNN model underestimated the canopy interception by 29.2% in two points and overestimated it by 21.7% in another two points (Figure 5). The canopy water interception depends on the leaf area in the canopy and therefore is closely related to LAI and NDVI. Assuming the water interception rate per unit leaf area in the canopy is the same, the total canopy interception could be linearly related to LAI. In the winter wheat field in this study, NDVI is increasing with the LAI increasing and reached the maximum of approximately 0.9 when LAI ranges from 4 to 7 (Figure 6), which is called saturation of the NDVI [65]. NDVI saturation at high LAI values significantly impacts LAI results. As LAI increases, NDVI may reach a maximum and cease to respond proportionally, leading to an underestimation of actual LAI [66]. In deciduous canopies, the LAI of the stands may reach a large value, which saturates the NDVI [67], consequently resulting in a low correlation between NDVI and LAI. Therefore, when the canopy interception is high (>1.4 mm) with a large LAI (4–6), the NDVI cannot sensitively reflect the change in LAI and consequently cause a large error in canopy interception estimation. The 6 large canopy interceptions from 1.48 to 1.80 mm (data in circle in Figure 4) were observed in LAI from 4.48 to 5.95, while the corresponding NDVI varied from 0.875 to 0.908. The smaller changes in NDVI (0.875–0.908) and $R_{\triangle NDVI}$ (0.056–0.096) compared to the larger change in LAI (4.48–5.95) finally induce a large error

in canopy interception estimation by the three methods for canopy interception higher than 1.4 mm and LAI larger than 4.0 (Figures 3–5).
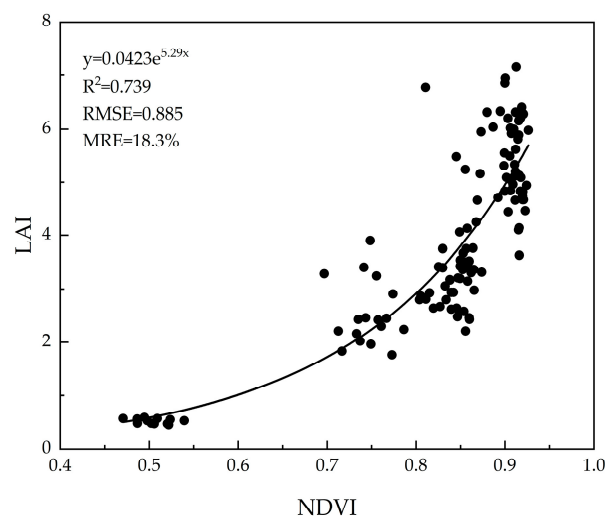
Figure 6. The relationship between normalized difference vegetation index (NDVI) and leaf area index (LAI) in winter wheat.

5. Conclusions

The vegetative indices of winter wheat canopy before and after sprinkler irrigation were determined by the UAV image data in two winter wheat seasons and then used to develop a canopy interception model by three methods. Main conclusions drawn are as follows.

1. The canopy water interception of winter wheat under sprinkler irrigation conditions averaged 0.63 mm for an LAI range of 4–6 in the wheat heading and grain-filling stages.
2. Canopy water interception is first significantly ($p < 0.05$) related to $R_{\triangle NDVI}$, and secondly related to indices of Blue, Nir, TGDVI, DVI, NDRE, and SAVI.
3. Linear regression models performed well to estimate canopy water interception; however, RF models and BPNN models underestimated canopy interception due to the saturation of NDVI for large LAI (>4).
4. The UAV technology combined with linear regression models is recommended for estimating canopy water interception of plants.

Author Contributions: Conception and design of experiments: H.L.; performance of experiments and analysis of data: X.Z. and L.L.; writing—review and editing: H.L. and X.Z. All authors have read and agreed to the published version of the manuscript.

Data Availability Statement: Data sharing is not applicable to this article.

Conflicts of Interest: The authors declare no conflict of interest.

References

1. Han, X.; Wang, L.; Wang, Y. Canopy interception of summer corn and its influencing factors under natural rainfall. *Sci. Agric. Sin.* **2014**, *47*, 1541–1549.
2. Llorens, P.; Domingo, F. Rainfall partitioning by vegetation under Mediterranean conditions. A review of studies in Europe. *J. Hydrol.* **2007**, *335*, 37–54. [CrossRef]

3. Grunicke, S.; Queck, R.; Bernhofer, C. Long-term investigation of forest canopy rainfall interception for a spruce stand. *Agric. For. Meteorol.* **2020**, *292*, 108125. [CrossRef]

4. Lull, H.W. Ecological and silvicultural aspects. In *Handbook of Applied Hydrology*; Chow, V.T., Ed.; McGraw-Hill: New York, NY, USA, 1964.

5. Ma, Y.; Gao, S.; Li, X.; Lu, R.; Zhang, S.; Li, G. Rainfall canopy partitioning and its influencing factors of riparian shrub in the alpine region. *J. Desert Res.* **2012**, *32*, 963–971.

6. China, National Bureau of Statistics. *National Statistics Yearbook*; China Statistics Press: Beijing, China, 2023.

7. Liu, C.M.; Zhang, X.Y.; Zhang, Y.Q. Determination of daily evaporation and evapotranspiration of winter wheat and maize by large-scale weighing lysimeter and micro-lysimeter. *Agric. For. Meteorol.* **2002**, *111*, 109–120. [CrossRef]

8. Liu, H.J.; Kang, Y.H.; Yao, S.M.; Sun, Z.Q.; Liu, S.P.; Wang, Q.G. Field evaluation on water productivity of winter wheat under sprinkler or surface irrigation in the north china plain. *Irrig. Drain* **2013**, *62*, 37–49. [CrossRef]

9. Yan, H.J.; Hui, X.; Li, M.N.; Xu, Y.C. Development in sprinkler irrigation technology in China. *Irrig. Drain* **2020**, *69*, 75–87. [CrossRef]

10. Kang, Y.H.; Wang, Q.G.; Liu, H.J. Winter wheat canopy interception and its influence factors under sprinkler irrigation. *Agric. Water Manag.* **2005**, *74*, 189–199. [CrossRef]

11. Tang, X.P.; Liu, H.J.; Yang, L.; Li, L.; Chang, J. Energy balance, microclimate, and crop evapotranspiration of winter wheat (*Triticum aestivum* L.) under sprinkler irrigation. *Agriculture* **2022**, *12*, 953. [CrossRef]

12. Liu, H.J.; Kang, Y.H. Effect of sprinkler irrigation on microclimate in the winter wheat field in the North China Plain. *Agric. Water Manag.* **2006**, *84*, 3–19. [CrossRef]

13. Urrego-Pereira, Y.; Cavero, J.; Medina, E.T.; Martínez-Cob, A. Microclimatic and physiological changes under a center pivot system irrigating maize. *Agric. Water Manag.* **2013**, *119*, 19–31. [CrossRef]

14. Urrego-Pereira, Y.; Cavero, J.; Medina, E.T.; Martínez-Cob, A. Role of transpiration reduction during center-pivot sprinkler irrigation in application efficiency. *J. Irrig. Drain Eng.* **2013**, *139*, 221–232. [CrossRef]

15. Du, Y.; Wang, J.; Liu, Z.; Cai, C.; Yang, J.; Gan, Z. Water distribution and microclimatic effects of sprinkler irrigation on spring wheat field. *Chin. J. Appl. Ecol.* **2001**, *12*, 398–400.

16. Zhu, Z.; Zhu, D.; Ge, M. Effects of irrigation characteristics and plant morphological features on interception of sprinkler water by maize plants. *Irrig. Sci.* **2023**, *41*, 337–353. [CrossRef]

17. Wang, J.; Liu, Y.; Li, B.; Li, Z.; Zhang, Y.; Zhang, S.; Pan, Y.; Zhang, F. The throughfall, stemflow, and canopy interception loss in corn and soybean fields in northeast China. *Water* **2024**, *16*, 253. [CrossRef]

18. Liu, H.J.; Chang, J.; Tang, X.P.; Zhang, J.P. In situ measurement of stemflow, throughfall and canopy interception of sprinkler irrigation water in a wheat field. *Agriculture* **2022**, *12*, 1265. [CrossRef]

19. Eskandari, R.; Mahdianpari, M.; Mohammadimanesh, F.; Salehi, B.; Brisco, B.; Homayouni, S. Meta-analysis of unmanned aerial vehicle (UAV) imagery for agro-environmental monitoring using machine learning and statistical models. *Remote Sens.* **2020**, *12*, 3511. [CrossRef]

20. Pádua, L.; Vanko, J.; Hruska, J.; Adao, T.; Sousa, J.J.; Peres, E.; Morais, R. UAS, sensors, and data processing in agroforestry: A review towards practical applications. *Int. J. Remote Sens.* **2017**, *38*, 2349–2391. [CrossRef]

21. Wang, Q.; Che, Y.; Chai, H.; Shao, K.; Yu, C.; Li, B.; Ma, Y. Monitoring of sugar beet growth using canopy spectrum and structural characteristics with UAV images. *Trans. Chin. Soc. Agric. Eng.* **2021**, *37*, 90–98.

22. Shi, B.; Yuan, Y.; Zhuang, T.; Xu, X.; Schmidhalter, U.; Ata-Ui-Karim, S.T.; Zhao, B.; Liu, X.; Tian, Y.; Zhu, Y.; et al. Improving water status prediction of winter wheat using multi-source data with machine learning. *Eur. J. Agron.* **2022**, *139*, 126548. [CrossRef]

23. Shi, H.Z.; Guo, J.J.; An, J.Q.; Tang, Z.J.; Wang, X.; Li, W.Y.; Zhao, X.; Jin, L.; Xiang, Y.Z.; Li, Z.J.; et al. Estimation of chlorophyll content in soybean crop at different growth stages based on optimal spectral index. *Agronomy* **2023**, *13*, 663. [CrossRef]

24. Ceccato, P.; Flasse, S.; Tarantola, S.; Jacquemoud, S.; Grégoire, J.M. Detecting vegetation leaf water content using reflectance in the optical domain. *Remote Sens. Environ.* **2001**, *77*, 22–33. [CrossRef]

25. Mobasheri, M.R.; Fatemi, S.B. Leaf equivalent water Thickness assessment using reflectance at optimum wavelengths. *Theor. Exp. Plant Physiol.* **2013**, *25*, 196–202. [CrossRef]

26. Liu, L.; Zhang, S.; Zhang, B. Evaluation of hyperspectral indices for retrieval of canopy equivalent water thickness and gravimetric water content. *Int. J. Remote Sens.* **2016**, *37*, 3384–3399. [CrossRef]

27. Oliveira, S.; Cunha, J.; Nóbrega, R.L.B.; Gash, J.H.; Valente, F. Enhancing global rainfall interception loss estimation through vegetation structure modeling. *J. Hydrol.* **2024**, *631*, 130672. [CrossRef]

28. Abdukeram, A.; Abudureyimu, A.; Xiao, Z.; Liu, S.; Bilali, Y.; Mamt, M.; Yiming, M. Experimental study on snow interception of Picea schrenkiana canopy based on UAV images. *J. Arid. Land Resour. Environ.* **2022**, *36*, 163–170.

29. Bulcock, H.H.; Jewitt, G.P.W. Spatial mapping of leaf area index using hyperspectral remote sensing for hydrological applications with a particular focus on canopy interception. *Hydrol. Earth Syst. Sci.* **2010**, *14*, 383–392. [CrossRef]

30. Zhang, X.W.; Zhang, K.F.; Wu, S.Q.; Shi, H.T.; Sun, Y.Q.; Zhao, Y.D.; Fu, E.J.; Chen, S.; Bian, C.F.; Ban, W. An investigation of winter wheat leaf area index fitting model using spectral and canopy height model data from unmanned aerial vehicle imagery. *Remote Sens.* **2022**, *14*, 5087. [CrossRef]

31. Liu, Y.; Wang, F.; Zhang, S.; Ding, W.; Li, R.; Han, J.; Ge, W.; Chen, H.; Shi, S. Analysis of canopy interception characteristics and influencing factors in typical artificial forest in the Loess Plateau semi-arid region. *J. Environ. Manag.* **2024**, *370*, 122455. [CrossRef] [PubMed]

32. Wang, L.A.; Zhou, X.D.; Zhu, X.K.; Dong, Z.D.; Guo, W.S. Estimation of biomass in wheat using random forest regression algorithm and remote sensing data. *Crop J.* **2016**, *4*, 212–219. [CrossRef]

33. Li, L.; Liu, H.; Gao, Z.; Yang, L.; Feng, D. Soil evaporation and its influencingfactors under poplar shelterbelts. *Bull. Soil Water Conserv.* **2021**, *41*, 82–88.

34. Yang, F.; Jiang, Y.; Li, H.; Hui, X.; Xing, S.C. Accurate model development for predicting sprinkler water distribution on undulating and mountainous terrain. *Comput. Electron. Agric.* **2024**, *224*, 109196. [CrossRef]

35. Li, J.S. Modeling crop yield as affected by uniformity of sprinkler irrigation system. *Agric. Water Manag.* **1998**, *38*, 135–146. [CrossRef]

36. Bard, A.E.; Bakeer, G.A.; EL-Tantawy, M.T.; Awwad, A.H. Sprinkler and trickle irrigations affected by climatic conditions in upper Egypt. *Irrig. Drain* **2006**, *23*, 346–361.

37. Cheng, Q.; Ding, F.; Xu, H.G.; Guo, S.Z.; Li, Z.P.; Chen, Z. Quantifying corn LAI using machine learning and UAV multispectral imaging. *Precis. Agric.* **2024**, *25*, 1777–1799. [CrossRef]

38. Pan, F.; Guo, J.; Miao, J.; Xu, H.; Tian, B.; Gong, D.; Zhao, J.; Lan, Y. Summer maize LAI retrieval based on multi-source remote sensing data. *Int. J. Agric. Biol. Eng.* **2023**, *16*, 179–186. [CrossRef]

39. Chen, P.; Liang, F. Cotton nitrogen nutrition diagnosis based on spectrum and texture feature of images from low altitude unmanned aerial vehicle. *Sci. Agric. Sin.* **2019**, *52*, 2220–2229.

40. Yu, J.; Zhang, Y.; Song, Z.; Jiang, D.; Guo, Y.; Liu, Y.; Chang, Q. Estimating leaf area index in apple orchard by UAV multispectral images with spectral and texture information. *Remote Sens.* **2024**, *16*, 3237. [CrossRef]

41. Rouse, J.W.; Haas, R.H.; Deering, D.W.; Schell, J.A. *Monitoring the Vernal Advancement and Retrogradation (Green Wave Effect) of Natural Vegetation*; No. NASA-CR-132982; NASA: Washington, DC, USA, 1973.

42. Wang, F.; Wang, K.; Li, S.; Chen, B.; Chen, J. Estimation of chlorophyll and nitrogen contents in cotton leaves using digital camera and imaging spectrometer. *Acta Agron. Sin.* **2010**, *36*, 1981–1989.

43. Fitzgerald, G.; Rodriguez, D.; O'Leary, G. Measuring and predicting canopy nitrogen nutrition in wheat using a spectral index—The canopy chlorophyll content index (CCCI). *Field Crops Res.* **2010**, *116*, 318–324. [CrossRef]

44. Huete, A.R. A soil-adjusted vegetation index (SAVI). *Remote Sens. Environ.* **1988**, *25*, 295–309. [CrossRef]

45. Tang, S.H.; Zhu, Q.J.; Shuai, Y.M.; Xie, D.H.; Zhou, G.L. A new vegetation index and its principle and application. In Proceedings of the 23rd International Geoscience and Remote Sensing Symposium (IGARSS 2003), Toulouse, France, 21–25 July 2003; IEEE: New York, NY, USA, 2003; pp. 2060–2062.

46. McFeeters, S.K. The use of the normalized difference water index (NDWI) in the delineation of open water features. *Int. J. Remote Sens.* **1996**, *17*, 1425–1432. [CrossRef]

47. Gong, R.X.; Zhang, H.A.; Lu, X.H.; Wan, H.L.; Zhang, Y.; Luo, X.; Zhang, J.; Xie, R.X. An integrated UAV growth monitoring model of Cinnamomum camphora based on whale optimization algorithm. *PLoS ONE* **2024**, *19*, 21. [CrossRef] [PubMed]

48. Korkmaz, M. A study over the general formula of regression sum of squares in multiple linear regression. *Numer. Meth. Part Differ. Equ.* **2021**, *37*, 406–421. [CrossRef]

49. Dou, J.; Xiang, Z.; Xu, Q.; Zheng, P.; Wang, X.; Su, A.; Liu, J.; Luo, W. Application and development trend of machine learning in landslide intelligent disaster prevention and mitigation. *Earth Sci.* **2023**, *48*, 1657–1674.

50. Ceh, M.; Kilibarda, M.; Lisec, A.; Bajat, B. Estimating the performance of random forest versus multiple regression for predicting prices of the apartments. *ISPRS Int. J. Geoinf.* **2018**, *7*, 168. [CrossRef]

51. Jin, C.; Jin, S.W.; Qin, L.N. Attribute selection method based on a hybrid BPNN and PSO algorithms. *Appl. Soft Comput.* **2012**, *12*, 2147–2155. [CrossRef]

52. Xia, K.; Li, C.; Shen, J. An optimization algorithm on the number of hidden layer nodes in feed-forward neural network. *Comput. Sci.* **2005**, *32*, 143–145.

53. Xiang, Y.; An, J.; Zhao, X.; Jin, L.; Li, Z.; Zhang, F. Soybean growth parameters and yield estimation based on UAV multispectral remote sensing. *Trans. Chin. Soc. Agric. Mac.* **2023**, *54*, 230–239.

54. Cohen, J. *Statistical Power Analysis for the Behavioral Sciences, 2nd ed*; Routledge: New York, 1988.

55. Li, J.S.; Rao, M.J. Sprinkler water distributions as affected by winter wheat canopy. *Irrig. Sci.* **2000**, *20*, 29–35. [CrossRef]

56. Li, H.; Guo, X.; Chen, R.; Wang, J. Effects of sprinkler uniformity and irrigation volume on the water distribution below the canopy of winter wheat. *Trans. Chin. Soc. Agric. Eng.* **2021**, *37*, 102–111.

57. Yang, Q.; Lai, F.; He, J.; Wei, Q.; Wang, W.; Wan, P.; Fu, Q. Hyperspectral properties of rice varieties with varying resistance under brown planthopper (nilaparvata lugens) infestation. *Chin. J. Rice Sci.* **2024**, *38*, 81–90.

58. Nagler, P.L.; Glenn, E.P.; Lewis Thompson, T.; Huete, A. Leaf area index and normalized difference vegetation index as predictors of canopy characteristics and light interception by riparian species on the Lower Colorado River. *Agric. For. Meteorol.* **2004**, *125*, 1–17. [CrossRef]

59. Han, X.; Wei, Z.; Chen, H.; Zhang, B.Z.; Li, Y.N.; Du, T.S. Inversion of winter wheat growth parameters and yield under different water treatments based on UAV multispectral remote sensing. *Front. Plant Sci.* **2021**, *12*, 13. [CrossRef] [PubMed]

60. Kim, N.; Ha, K.-J.; Park, N.-W.; Cho, J.; Hong, S.; Lee, Y.-W. A comparison between major artificial Intelligence models for crop yield prediction: Case study of the midwestern United States, 2006–2015. *ISPRS Int. J. Geoinf.* **2019**, *8*, 240. [CrossRef]

61. Wang, T.L.; Gao, M.F.; Cao, C.L.; You, J.; Zhang, X.W.; Shen, L.Z. Winter wheat chlorophyll content retrieval based on machine learning using in situ hyperspectral data. *Comput. Electron. Agric.* **2022**, *193*, 106728. [CrossRef]

62. Yu, N.; Li, L.J.; Schmitz, N.; Tiaz, L.F.; Greenberg, J.A.; Diers, B.W. Development of methods to improve soybean yield estimation and predict plant maturity with an unmanned aerial vehicle based platform. *Remote Sens. Environ.* **2016**, *187*, 91–101. [CrossRef]

63. Elsherbiny, O.; Fan, Y.Y.; Zhou, L.; Qiu, Z.J. Fusion of feature selection methods and regression algorithms for predicting the canopy water content of rice based on hyperspectral data. *Agriculture* **2021**, *11*, 51. [CrossRef]

64. Dong, Y.; Zhang, Q. A survey of depth semantic feature extraction of high-resolution remote sensing images based on CNN. *Remote Sens. Technol. Appl.* **2019**, *34*, 1–11.

65. Crockford, R.H.; Richardson, D.P. Partitioning of rainfall into throughfall, stemflow and interception: Effect of forest type, ground cover and climate. *Hydrol. Process.* **2000**, *14*, 2903–2920. [CrossRef]

66. Wang, Q.; Adiku, S.; Tenhunen, J.; Granier, A. On the relationship of NDVI with leaf area index in a deciduous forest site. *Remote Sens. Environ.* **2005**, *94*, 244–255. [CrossRef]

67. Birky, A.K. NDVI and a simple model of deciduous forest seasonal dynamics. *Ecol. Model.* **2001**, *143*, 43–58. [CrossRef]